zMADM (zebrafish mosaic analysis with double markers) for single-cell gene knockout and dual-lineage tracing

Bing Xu[a,b,1], Sarah Kucenas[c], and Hui Zong[a,b,1]

[a]Department of Microbiology, Immunology, and Cancer Biology, University of Virginia, Charlottesville, VA 22908; [b]Cancer Center, University of Virginia, Charlottesville, VA 22908; and [c]Department of Biology, University of Virginia, Charlottesville, VA 22908

Edited by Lalita Ramakrishnan, Molecular Immunity Unit, Department of Medicine, University of Cambridge, Cambridge, United Kingdom; received December 13, 2021; accepted January 23, 2022

As a vertebrate model organism, zebrafish has many unique advantages in developmental studies, regenerative biology, and disease modeling. However, tissue-specific gene knockout in zebrafish is challenging due to technical difficulties in making floxed alleles. Even when successful, tissue-level knockout can affect too many cells, making it difficult to distinguish cell autonomous from noncell autonomous gene function. Here, we present a genetic system termed zebrafish mosaic analysis with double markers (zMADM). Through Cre/loxP-mediated interchromosomal mitotic recombination of two reciprocally chimeric fluorescent genes, zMADM generates sporadic (<0.5%), GFP$^+$ mutant cells along with RFP$^+$ sibling wild-type cells, enabling phenotypic analysis at single-cell resolution. Using wild-type zMADM, we traced two sibling cells (GFP$^+$ and RFP$^+$) in real time during a dynamic developmental process. Using *nf1* mutant zMADM, we demonstrated an overproliferation phenotype of *nf1* mutant cells in comparison to wild-type sibling cells in the same zebrafish. The readiness of zMADM to produce sporadic mutant cells without the need to generate floxed alleles should fundamentally improve the throughput of genetic analysis in zebrafish; the lineage-tracing capability combined with phenotypic analysis at the single-cell level should lead to deep insights into developmental and disease mechanisms. Therefore, we are confident that zMADM will enable groundbreaking discoveries once broadly distributed in the field.

zebrafish | mosaic analysis with double markers | lineage tracing | single-cell gene knockout

Zebrafish as a model organism has multiple advantages, including high fecundity, external and fast development of embryos, and embryonic transparency, enabling in vivo, real-time analysis (1), and has been broadly used for studying developmental processes and modeling human disease (2). Recently developed methods for efficient genetic manipulation, including zinc finger endonucleases (ZFNs), transcription activator-like effector nucleases (TALENs), and CRISPR/CRISPR-associated 9 (Cas9), have further facilitated the delineation of gene function during normal development and in disease (3). However, to distinguish cell autonomous gene functions, one must rely on genetic mosaics, in which a few mutant cells coexist with wild-type cells in the same tissue. While cell transplantation is commonly used, its labor intensiveness has motivated the recent development of tissue-specific conditional knockout (CKO) techniques via nonhomologous end-joining–mediated knock-in (4–7). While powerful, current CKO strategies are still labor intensive and tend to generate an overwhelming number of mutant cells. Furthermore, fluorescent labeling of mutant cells could be lost if the endogenous promoter for the targeted gene shuts down later in development. Therefore, the development of a genetic system that combines unequivocal fluorescent labeling and gene knockout at the single-cell level would greatly empower the zebrafish model to provide unprecedented insights into genetic control of cellular behaviors during development and disease.

Mosaic analysis with a repressible cell marker (MARCM) and mosaic analysis with double markers (MADM) were developed in *Drosophila* and mice, respectively, to create genetic mosaics (8–10). Through recombinase-mediated interchromosomal mitotic recombination, these systems generate sparse and unequivocally labeled mutant cells along with sibling wild-type cells labeled with another color, enabling cellular-resolution phenotypic analysis of gene function in complex biological processes. Both MARCM and MADM are broadly adopted in many fields, including neuroscience (11–13), developmental biology (14, 15), and cancer biology (16–18). We envision that real-time, in vivo imaging analysis with MADM in zebrafish could reveal even more intricate details of developmental processes and disease mechanisms. Furthermore, once zebrafish MADM (zMADM) is built on one chromosome, by design all genes between the zMADM locus and the telomere on that chromosome arm can be studied using simple CRISPR/Cas9-induced mutagenesis without the need of making floxed alleles (9, 19), saving tremendous time and effort. Here, we describe the establishment and characterization of zMADM and showcase its applications for dual-lineage tracing and mutant phenotypic analysis at the single-cell resolution.

Results

The Design Scheme of zMADM. zMADM consists of two cassettes of reciprocally chimeric fluorescent genes driven by a ubiquitously expressed strong promoter, which are separately knocked into the

Significance

The transparent body of the larval zebrafish makes it an excellent vertebrate model for studying both developmental and disease processes in real time. However, the difficulty of genetic manipulation of zebrafish has greatly hindered its full power in biological studies. To overcome these hurdles, we establish a genetic system called zebrafish mosaic analysis with double markers (zMADM). zMADM has three unique advantages: First, it can achieve conditional knockout of genes residing on the zMADM-bearing chromosome without the need to generate floxed alleles, which is highly challenging and time consuming in the zebrafish; second, it allows the fate mapping of two sibling lineages; and third, it enables cell autonomous phenotypic analysis at single-cell resolution with sibling wild-type cells as internal control.

Author contributions: B.X. and H.Z. designed research; B.X. performed research; B.X., S.K., and H.Z. analyzed data; and B.X., S.K., and H.Z. wrote the paper.

The authors declare no competing interest.

This article is a PNAS Direct Submission.

[1]To whom correspondence may be addressed. Email: bx2u@virginia.edu or hz9s@virginia.edu.

This article contains supporting information online at http://www.pnas.org/lookup/suppl/doi:10.1073/pnas.2122529119/-/DCSupplemental.

Published February 23, 2022.

identical genomic locus of homologous chromosomes and then bred together. While cells in zMADM lack fluorescent protein expression in the absence of Cre recombinase, they can be labeled by GFP or RFP via Cre-mediated interchromosomal recombination at the G2 phase after DNA replication (Fig. 1*A*): If the recombined chromosomes are separated into different daughter cells (X segregation), one daughter cell becomes green and the other red; however, if the recombined chromosomes are cosegregated into the same daughter cell (Z segregation), one daughter cell becomes yellow while the other remains colorless. It should be noted that the low probability of interchromosomal recombination enables sporadic labeling of single cells.

If a mutant gene is located between a zMADM cassette and the telomere, G2/X segregation will generate a green, homozygous mutant cell and a sibling red, wild-type cell from a heterozygous mother cell, while G2/Z segregation will generate a yellow, heterozygous cell (Fig. 1*A*). It should be noted that, in nondividing cells (G0/G1), Cre can also mediate recombination to produce yellow, heterozygous cells (Fig. 1*B*). Therefore, in a single zebrafish, zMADM can sporadically generate homozygous, heterozygous, and wild-type cells from the same lineage and label them with GFP, GFP/RFP, and RFP, respectively.

Construction of zMADM Cassettes. To ensure high-level expression of fluorescent genes from a single copy of the zMADM cassette for live imaging, we first screened for a strong promoter and a bright RFP in zebrafish. For promoter choice, we compared the intensity of eGFP driven by two commonly used ubiquitous promoters, zebrafish ubiquitin promoter (*zubi*) (20) and the *eab2* promoter (21) by transiently injecting either *zubi:eGFP* or *eab2:eGFP* plasmids, and found that the *eab2* promoter was significantly stronger (Fig. 1 *C* and *E*). To identify the strongest RFP in zebrafish, we compared the intensity of five commonly used RFPs, including mApple, mRuby2, mRuby3, TagRFP, and mScarlet by transiently injecting messenger RNA (mRNA) encoding these distinct RFPs, and found that mApple was the brightest among them (Fig. 1 *D* and *F*). mApple is derived from DsRed (22) and has been used for making transgenic zebrafish lines (23). Although it is not the brightest RFP in mammalian cells (22), it turned out to be brighter than other commonly used RFPs in zebrafish.

Because zMADM requires the insertion of a loxP-containing intron into the coding sequence (CDS) of fluorescent proteins, we inserted an artificial β-globin intron containing loxP sites into the CDS of eGFP and mApple, abiding by the exon–intron boundary consensus sequence (*SI Appendix*, Fig. S1). Next, we verified that N-eGFP:intron:C-eGFP (termed GG) and N-mApple:intron:C-mApple (termed AA) could be correctly spliced and translated into functional eGFP and mApple in zebrafish (Fig. 1 *G* and *H*). Finally, to test whether the Cre/loxP system could mediate in trans recombination in zebrafish, we constructed N-eGFP:intron:C-mApple (GA) and N-mApple:intron:C-eGFP (AG) plasmids (Fig. 1*I* and *SI Appendix*, Fig. S1) and coinjected them with *Cre* mRNA into one-cell zebrafish embryos. Green and red fluorescent signals were seen in zebrafish larvae at 3 d postfertilization (dpf) with *Cre* but not in control larvae (Fig. 1*J*), indicating successful interplasmid recombination mediated by Cre/loxP.

CRISPR/Cas9-Mediated Knock-in of zMADM Cassettes. To generate stable zMADM alleles, we used three criteria to select a suitable genomic locus for knocking in the MADM cassettes. First, we focused our search between the centromere and our gene of interest (in this case *nf1b*) because only the genes between the zMADM cassette and the telomere can be studied. Second, we chose intergenic regions to ensure that the insertion of zMADM cassettes would not disrupt the expression of endogenous genes. Third, we tried our best to find a locus near housekeeping genes to ensure robust expression of fluorescent proteins encoded by zMADM. According to these criteria, we identified an intergenic region between *rassf2b* and *kcnip3b* on zebrafish chromosome 10. To ensure efficient targeting, we designed five single-guide RNAs (sgRNAs), injected each of them with Cas9 protein into zebrafish embryos, and identified sgRNA-3 as the one with the highest DNA cutting efficiency (*SI Appendix*, Fig. S2). Finally, we constructed donor plasmids containing the zMADM cassettes and a 500-bp homology arm containing the sgRNA target sequence (*SI Appendix*, Fig. S3*A*). We coinjected donor plasmids (donor *eab2:GA* or donor *eab2:AG*) with *zCas9* (24) mRNA and sgRNA into one-cell zebrafish embryos and raised them to adulthood. After breeding each putative founder with wild-type zebrafish, we used two pairs of primers to screen their progeny for successful knock-in (*SI Appendix*, Fig. S3 *A* and *B*) and found 1 zMADM-AG and 2 zMADM-GA germline founders from 56 *eab2:AG*- and 195 *eab2:GA*-injected zebrafish (*SI Appendix*, Fig. S3*C*). After obtaining zMADM founders (*SI Appendix*, Fig. S3 *D* and *E*), we sequenced the 5′- and 3′-flanking regions of the insertion sites. The small indels we identified (*SI Appendix*, Fig. S3 *F* and *G*) should not interfere with the function of neighboring genes because the zMADM cassettes were knocked into an intergenic region. Further, we bred these founders to homozygosity and observed no detectable health issues, including fertility.

Basic Characterizations of zMADM. To determine whether interchromosomal recombination could occur efficiently in zMADM, we injected *Cre* mRNA or an *eab2:Cre* plasmid into one-cell stage AG/GA embryos obtained by intercrossing zMADM-AG and zMADM-GA founders and examined the larvae at 4 dpf. We found green, red, and yellow cells in both *Cre* mRNA and *eab2:Cre* plasmid-injected zMADM larvae, but no signal in control zMADM larvae without Cre recombinase (Fig. 2 *A*–*C*). These results demonstrate the successful establishment of the zMADM system.

To characterize key features of zMADM, we performed a series of follow-up experiments. First, we estimated the total labeling efficiency of zMADM to be ∼0.5% by dividing the number of labeled cells by the total cell number (DAPI) in brains of 4-dpf zebrafish (Fig. 2*D* and *SI Appendix*, Fig. S4). While different Cre constructs or transgenes could lead to slightly different labeling efficiencies, this range is sparse enough for phenotypic analysis at the single-cell resolution, comparable to mouse MADM (9). Second, according to the principle of zMADM, green and red cells should be generated simultaneously (Fig. 1*A*) and of equal number in wild-type zMADM larvae. *Cre* mRNA or *eab2:Cre* plasmid transiently injected zMADM larvae had no significant difference in the number of green and red cells (Fig. 2 *E* and *F*). Third, considering the time needed for Cre-mediated recombination and the expression/maturation of eGFP and mApple, we examined how early zMADM-labeled cells could be visualized and found that fluorescent signals could be clearly seen as early as 24 h postfertilization (hpf) in both *Cre* mRNA and *eab2:Cre* plasmid-injected zMADM embryos (Fig. 2 *G* and *H*). Additionally, we found that zMADM-labeled cells could still be visualized at 1.5 mo postfertilization (mpf), suggesting that the expression of fluorescent proteins persists under the *eab2* promoter (Fig. 2 *G* and *H*). Finally, we examined the cell types labeled in these experiments and found fine-branched neural cells in the brain, long muscle cells, vascular endothelial cells, epidermal cells, and cells in many other organs (Fig. 2 *I* and *J*), showcasing the single-cell resolution applicable to studies of cell morphologies and cell–cell interactions. To broadly apply zMADM for single-cell studies, we tested whether it could label specific cell types by *Cre* plasmids driven by specific promoters, such as neuronal or endothelial lineages. Using the *elavl3:Cre* plasmid, we

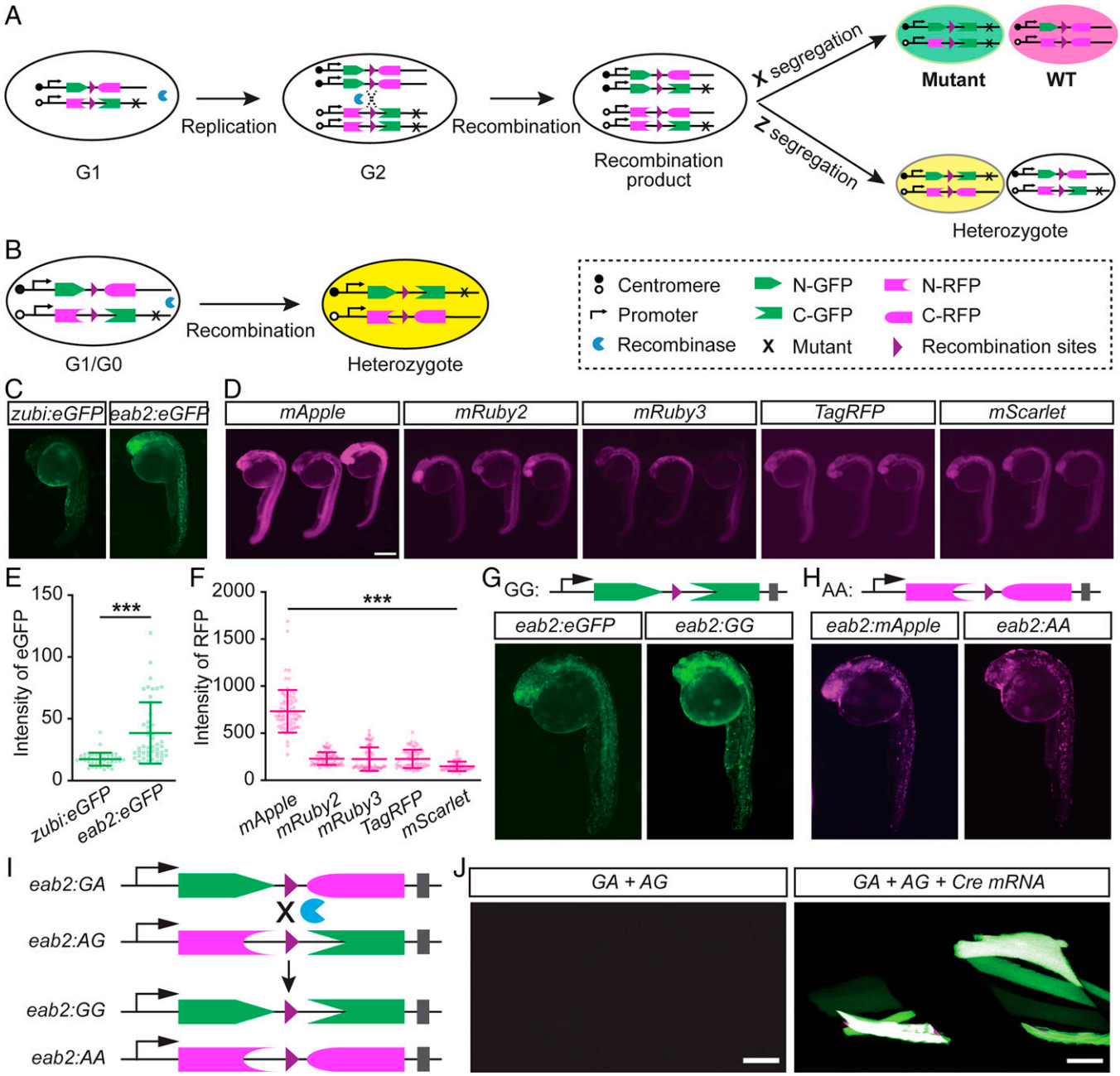

Fig. 1. Schematic of zMADM and comparative testing of genetic elements in zebrafish. (*A* and *B*) The schematic of zMADM in dividing (*A*) and nondividing (*B*) cells. In dividing cells (*A*), a colorless heterozygous cell generates a pair of green homozygous mutant and red wild-type cells via X segregation or one yellow and one colorless heterozygous cell via Z segregation. In nondividing cells (*B*), only yellow heterozygous cells are generated. (*C*) Representative images of 24-hpf embryos show the GFP signal in *eab2:eGFP*-injected zebrafish is stronger than that in *zubi:eGFP*-injected zebrafish. (*D*) Representative images of 24-hpf embryos show the red fluorescent signal in *mApple* mRNA-injected zebrafish is the brightest among the five RFPs tested. (Scale bars: 1.5 mm.) (*E*) Quantification of the GFP signal in *eab2:eGFP*- and *zubi:eGFP*-injected zebrafish. *zubi:eGFP*, $n = 46$; *eab2:eGFP*, $n = 47$. Data are mean ± SD, $^{***}P < 0.001$ (unpaired Student's *t* test). (*F*) Quantification of the red fluorescent signal in five RFP mRNA-injected zebrafish. (Scale bar: 2 mm.) *mApple*, $n = 76$; *mRuby2*, $n = 64$; *mRuby3*, $n = 67$; *TagRFP*, $n = 61$; *mScarlet*, $n = 47$. Data are mean ± SD, $^{***}P < 0.001$ (one-way ANOVA followed by Dunnett's multiple-comparisons test). (*G*) Schematics of *eab2:GG* and representative images of 24-hpf embryos show that *eab2:GG* produce eGFP signals to a level similar to that of the intact eGFP. (*H*) Schematics of *eab2:AA* and representative images of 24-hpf embryos show that *eab2:AA* produce mApple signals to a level similar to that of the intact mApple. (*I*) Schematics showing how Cre/loxP-mediated recombination between *eab2:GA* and *eab2:AG* plasmids generates *eab2:GG* and *eab2:AA*. (*J*) Representative confocal images of 3-dpf larvae when *eab2:GA* and *eab2:AG* plasmids were coinjected with or without *Cre* mRNA. (Scale bars: 35 μm.)

observed neurons in the brain labeled by zMADM, revealing fine neuronal processes (*SI Appendix*, Fig. S5*A*). Using the *kdrl:Cre* plasmid, we observed labeled endothelial cells, revealing single-cell morphology and branching patterns (*SI Appendix*, Fig. S5*B*). These results show zMADM can be used to label specific cell types by cell type-specific *Cre* plasmids.

Dual-Lineage Tracing with zMADM. Lineage tracing is a critical technique for revealing the developmental trajectory of stem/progenitor cells (25). Compared to previous methods, zMADM carries the unique advantage of labeling two daughter cells from a single mother cell with distinct colors, ideal for elucidating symmetric or asymmetric developmental patterns. After injecting *Cre* mRNA

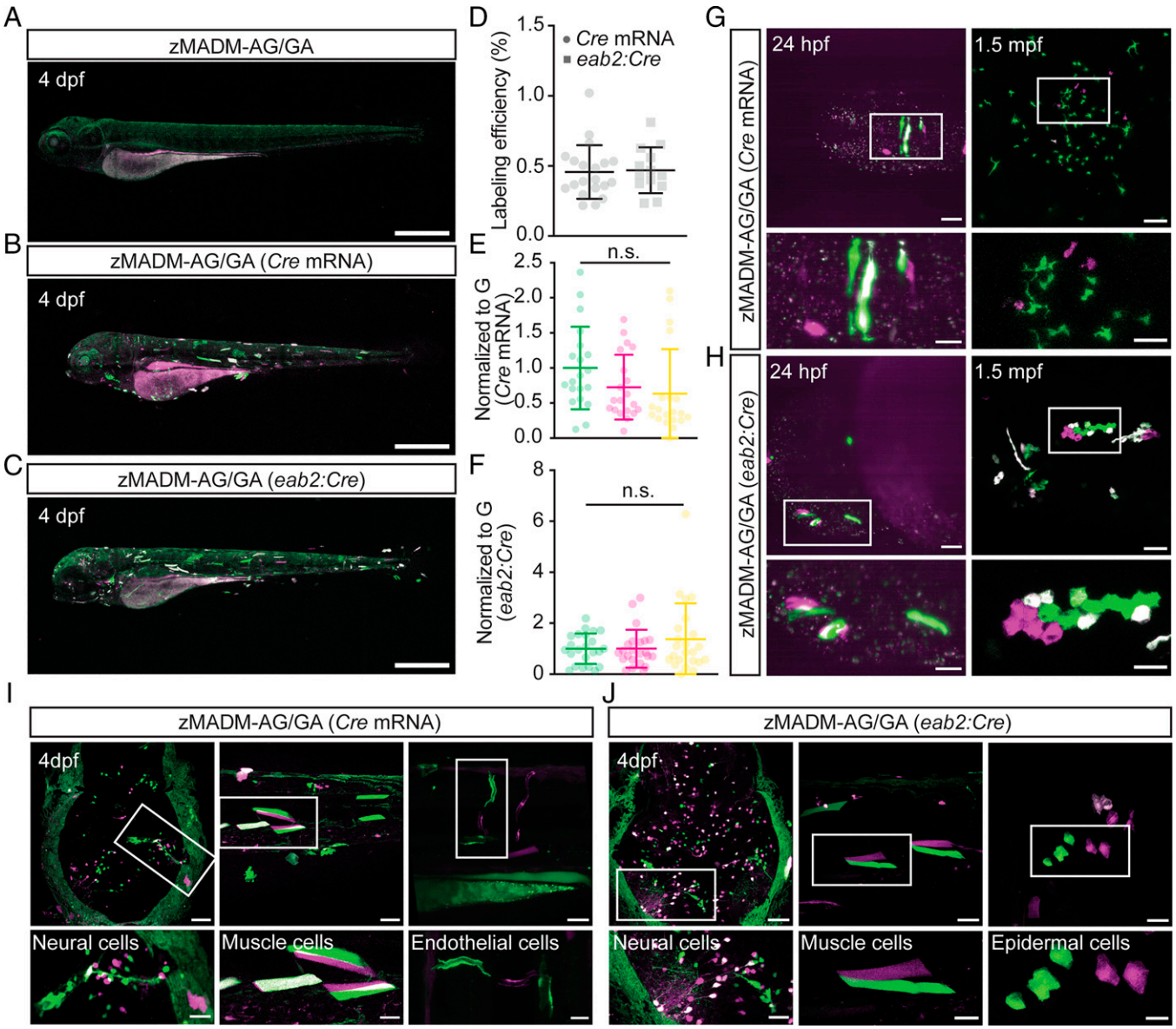

Fig. 2. Basic characterization of the zMADM system. (*A*–*C*) Representative confocal images of 4-dpf zMADM larvae showing that the injection of *Cre* mRNA (*B*) or *eab2:Cre* plasmid (*C*) results in fluorescent protein-labeled cells throughout the larvae, while there are no labeled cells in the absence of *Cre* (*A*). Note that the green signal in *A* is autofluorescence of zebrafish skin rather than eGFP expression. (Scale bars: 500 μm.) (*D*) Quantification of zMADM labeling efficiency shows that only ~0.5% total cells in zMADM larvae are labeled by the transient expression of Cre. *Cre* mRNA, $n = 20$; *eab2:Cre*, $n = 13$. Data are mean ± SD. (*E* and *F*) Labeling efficiency of green, red, and yellow cells normalized to green cell number in *Cre* mRNA-injected (*E*) or *eab2:Cre* plasmid-injected (*F*) zMADM zebrafish. $n = 20$. Data are mean ± SD. n.s., no significance (one-way ANOVA followed by Tukey's multiple-comparisons test). (*G* and *H*) Representative confocal images of 24-hpf and 1.5-mpf *Cre* mRNA-injected (*G*) or *eab2:Cre* plasmid-injected (*H*) zMADM larvae show that eGFP and mApple expression can be detected at an early embryonic stage and persist into adulthood. (Scale bars: *Upper*, 50 μm; *Lower*, 25 μm.) (*I*) Representative confocal images of 4 dpf *Cre* mRNA injected zMADM embryos show that zMADM can label multiple cell types. Scale bar: upper 50 μm, below 25 μm. (*J*) Representative confocal images of 4-dpf *eab2:Cre* plasmid-injected zMADM embryos show that zMADM can label multiple cell types. Note that the green signal surrounding the tissues in *I* and *J* is autofluorescence of zebrafish skin rather than eGFP expression. (Scale bars: *Upper*, 50 μm; *Lower*, 25 μm.)

into one-cell zMADM embryos, we imaged from 36 hpf onward. In four imaged brains, we found that the timing of appearance of labeled cells was stochastic, ranging between 36 and 53 hpf. In one example, we observed that green and red twin cells appeared around 38.5 hpf and then divided asynchronously (Fig. 3*A* and Movie S1). To determine the fate of zMADM-labeled progeny cells, we fixed the fish after live imaging and costained the fish with anti-DsRed antibody for mApple and anti-HuC/D antibody specific for neurons, revealing that both green- and red-labeled cells were neurons (Fig. 3 *B* and *C*). Therefore, the zMADM system, with its single-cell resolution and the ease of in vivo, time-lapse imaging, is a powerful tool for studying lineage development in detail.

Next, we used the zMADM system to study the dynamic process of neuronal column formation in the zebrafish optic tectum, which consists of tectal neurons tightly associated with the fibers of radial glial cells (26). Previous in vitro lineage studies demonstrated that mouse neural stem cells divide predominantly via asymmetric division during neurogenesis (27), and in vivo, two photon-imaging studies showed that many progeny die after birth in the mouse hippocampus (28). However, whether or not tectal neuronal column develops in a similar manner remains unknown. Because zMADM can clearly label twin daughter cells with two distinct colors, we hypothesized that different color patterns of neuronal columns could be found: 1) green and red columns side

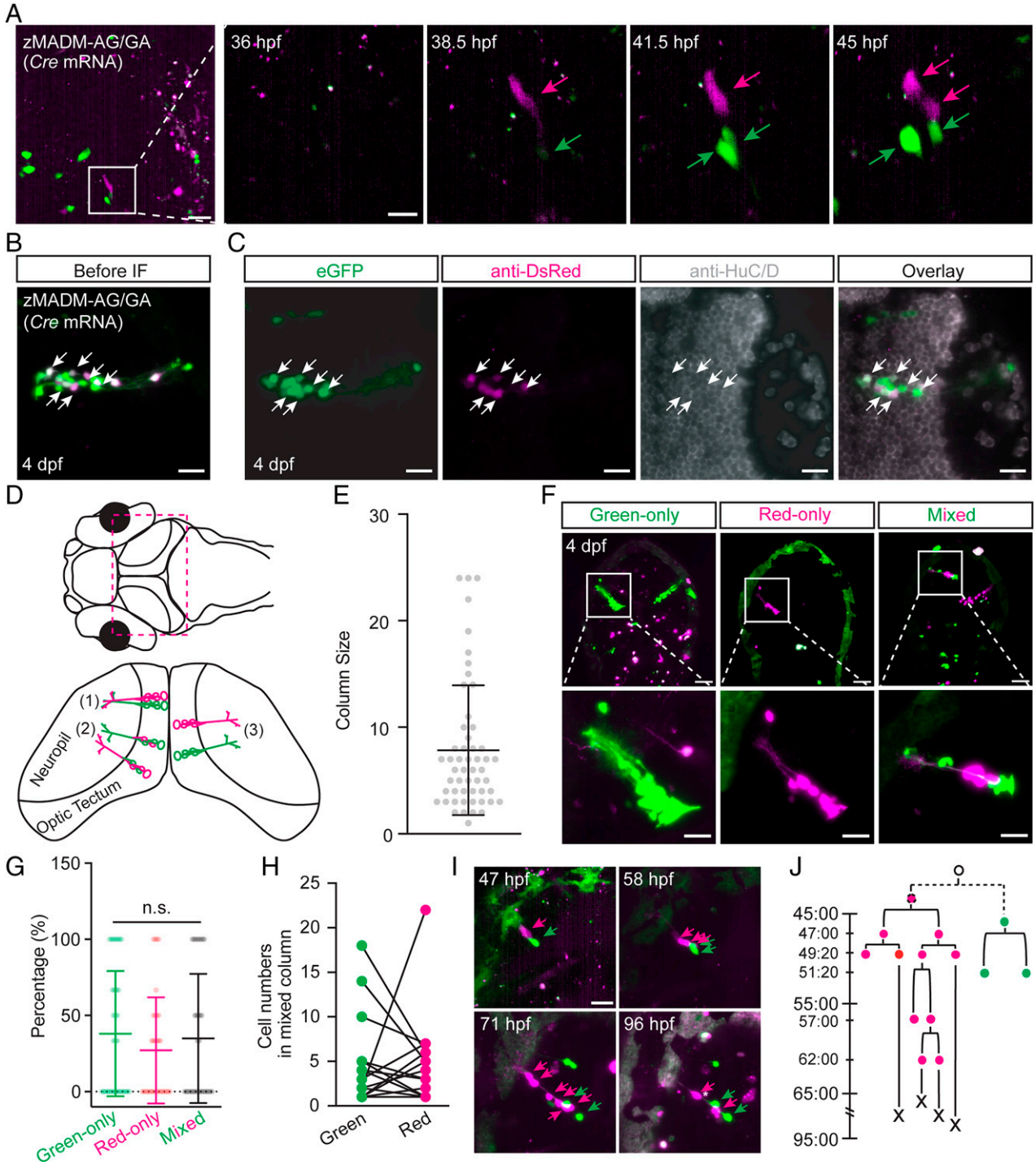

Fig. 3. Lineage tracing with the zMADM system. (*A*) Representative images from a time-lapse movie of *Cre* mRNA-mediated zMADM embryos from 36 hpf show that green and red twin cells are generated around 38.5 hpf from a colorless cell and continue to divide afterward. (Scale bars: *Left*, 25 μm; *Right*, 10 μm.) (*B*) Representative confocal image of 4-dpf zMADM-labeled brain cells before fixation. (Scale bar: 20 μm.) (*C*) The immunofluorescence of 4-dpf zMADM-labeled larvae with DsRed antibody for mApple and HuC/D antibody for neurons, indicating that immunofluorescence can be used to identify the cell type of zMADM-labeled cells. (Scale bar: 20 μm.) (*D*) Schematic of zMADM-labeled neuronal columns that can be generated from different division patterns of neural progenitor cells (see text for details). (*E*) The size of neuronal columns labeled by *eab2:Cre* plasmid-mediated zMADM is 7.8 ± 6.1. A total of 53 columns from 32 zebrafish were quantified. (*F*) Representative confocal images of green-only, red-only, and green and red cells mixed columns. (Scale bars: *Upper*, 50 μm; *Lower*, 20 μm.) (*G*) Quantification of the frequency of green-only, red-only, and mixed columns shows no difference among these three types of neuronal columns. $n = 32$. Data are mean ± SD. n.s., no significance (one-way ANOVA followed by Tukey's multiple-comparisons test). (*H*) Quantification of the numbers of green and red cells within each mixed neuronal column shows that the numbers of green and red cells are mostly different while the total numbers are similar. A total of 16 mixed columns from 14 zMADM zebrafish were quantified. (*I*) Representative time-lapse images of neuronal column formation. Sibling green and red cells went through multiple rounds of cell division to form the neuronal column, accompanied by some cell death events. The arrows indicate the neurons in the columns. The asterisk-labeled cells are cells from different optical layers. (Scale bar: 20 μm.) (*J*) The reconstructed lineage tree of neuronal column formation according to the time-lapse imaging of J. Most proliferative events occurred before 72 hpf. "X" marks the timing of cell death. The timescale on the left is labeled as hh:mm postfertilization.

by side with equal cell numbers, indicative of symmetric cell fate; 2) green and red cells interdigitated with different cell numbers, indicative of asymmetric cell fate; or 3) green only or red only columns, indicative of death of one of the twin zMADM-labeled cells after birth (Fig. 3*D*). We labeled the neuronal columns by transient expression of *eab2:Cre* plasmids in zMADM larvae. According to the morphology of the neuronal clusters, we identified and quantified a total of 53 neuronal columns from 32 larvae at 96 hpf and found the average cell number of zMADM-labeled columns was 7.8 ± 6.1 (mean ± SD) (Fig. 3*E*). When we examined the color pattern of these columns, we found three distinct types, green only, red only, or green and red mixed columns (Fig. 3*F*), but never observed symmetric columns, suggesting that neural progenitor cells (NPCs) divide asymmetrically during column formation. Furthermore, a large portion of single-colored columns demonstrate that one of the two sibling cells dies shortly after birth. In our data, we found the percentages of different zMADM-labeled neuronal columns were similar (green only, ~38.0 ± 41.1%; red only, ~27.1 ± 34.8%; mixed, ~34.9 ± 42.4%) (Fig. 3*G*), suggesting that the death rate of the progeny was ~65% (green only + red only: 38.0 + 27.1%). Furthermore, we found that the numbers of green and red cells in mixed columns were rarely equal (Fig. 3*H*), suggestive of asymmetric cell fate of two daughter cells that could result from different proliferative rate, different apoptotic rate, or both. In summary, we conclude that NPCs divide asymmetrically and that many progeny undergo apoptosis during tectal neuronal column formation.

Finally, to further explore the lineage dynamics during neuronal column formation, we performed a long-term, time-lapse imaging experiment from 47 to 96 hpf with a 20-min interval (Fig. 3*I* and Movie S2) and found that about 50% of the neurons in the columns died during imaging (Fig. 3 *I* and *J*), which is very close to the estimated death rate based on the analysis of fixed samples (Fig. 3*G*). Additionally, we found that the red progeny of this column proliferated much more than the green progeny, and this expansion occurred prior to 72 hpf, the time period when active neurogenesis happens and establishment of retinotopic organization occurs (29). After 72 hpf, the active death of many red cells led to equivalent numbers of green and red cells. In concordance with literature reports on the developmental wiring of zebrafish optic tectum, our observed high death rate after 72 hpf could be an active process of connectivity-based retinotopic organization: Retinal axons start entering the tectal neuropil at 60 hpf and by 72 hpf more than 50% of neurons show visual responses (29). In conclusion, this experiment demonstrated how real-time, dual-lineage tracing afforded by zMADM can help reveal dynamic developmental processes.

Single-Cell Knockout with zMADM. To examine whether zMADM could generate mutant and wild-type cells labeled with different colors for phenotypic analysis, we used *nf1* as a test case, which is a tumor suppressor gene that shuts down Ras guanosine triphosphatase (GTPases) by accelerating GTP hydrolysis (30, 31). Loss of *nf1* activates the Ras signaling pathway, promoting proliferation and survival, and leads to a variety of cancers (30). In zebrafish, there are two copies of *nf1*, *nf1a*, and *nf1b*, with redundant function (32). *nf1a* is located on chromosome 15, while *nf1b* is located on chromosome 10 where our zMADM cassettes reside. For this experiment, we performed a five-generation breeding scheme to recombine the *nf1b* mutant allele (ZFIN: ZDB-ALT-130528-3) with zMADM and to incorporate the *nf1a* mutant allele (ZFIN: ZDB-ALT-130528-1) as the background mutation (32) to generate zMADM-*nf1* zebrafish (*SI Appendix*, Fig. S6). When the *nf1b* mutant allele is recombined with the zMADM-AG allele, green cells will be *nf1* null and red cells will be wild type (Fig. 4*A*) (hereafter referred to as green zMADM-*nf1*). Compared to the wild-type zMADM, in which the green and red cell numbers are equal (green/red [G/R] ratio = 1) (Fig. 2*F*), we found that green *nf1* mutant cells outnumbered red wild-type cells in the brain, eye, and trunk of the green zMADM-*nf1* zebrafish (Fig. 4 *B–D*). Quantification demonstrated that G/R ratios are significantly higher than 1 in all of these three regions (brain, 2.986 ± 2.203; eye, 3.857 ± 2.975; trunk, 5.986 ± 4.525) (Fig. 4*E*). To control for the potential impact of fluorescent proteins on the cell proliferation and survival, we also established green zMADM-*nf1* by recombining the *nf1b* mutant allele with the zMADM-GA allele, in which red cells are *nf1* null (Fig. 4*F*), and found the same trend for cell numbers (brain, 4.210 ± 3.775; eye, 5.468 ± 4.250; trunk, 2.552 ± 2.468) (Fig. 4 *G–J*). These results demonstrate that, when combined with a mutant allele of interest, the zMADM system can label both mutant and wild-type cells in the same zebrafish to aid phenotypic analysis at single-cell resolution.

Discussion

Unique Advantages of zMADM in Comparison to Other Zebrafish Genetic Models. Here we establish a genetic system, zMADM, for mosaic analysis in zebrafish. Our work here complements previous zebrafish mosaic genetic models, including mosaic analysis in zebrafish (MAZe) and CKO models (4, 5, 33). MAZe uses a self-excising Cre to generate sporadic cells expressing Gal4, which in turn drives the expression of a gene of interest under the control of UAS, enabling mosaic analysis (33). Recent CKO models coupled with cell labeling involve two steps: first, knocking in sophisticatedly designed fluorescent gene-expressing cassettes flanked by loxP sites into the gene of interest, and second, upon Cre expression, the gene of interest and the original fluorescent gene are excised while a different fluorescent protein gets switched on, resulting in wild-type and knockout cells with different fluorescent proteins (4, 5). zMADM offers several unique advantages compared to these established approaches. First, MAZe is generally restricted to gain-of-function studies, whereas zMADM enables loss-of-function studies. Second, the expression level of fluorescent genes in CKO models is under the control of an endogenous promoter for the gene of interest, which could be insufficient or lacking if the progeny of CKO cells down-regulate or turn off the expression of the gene of interest. By contrast, fluorescent genes in zMADM are under the control of a strong, ubiquitous promoter that stays on throughout the lifetime of the zebrafish. Third, while CKO models generate mutant and wild-type cells stochastically, zMADM generates one mutant and one wild-type sibling cell from a single mother cell. Therefore, zMADM provides an ideal internal control to detect even the subtlest phenotypes through twin-spot comparison. Fourth, while conventional CKO methods that rely on in cis Cre recombination tend to affect too many cells to allow the distinguishing of cell autonomous from noncell autonomous gene functions, the sparseness of zMADM-labeled mutant cells generated through low-efficiency in trans Cre recombination enables phenotypic analysis of cell autonomous gene functions. Fifth, while the CKO methods require a labor-intensive setup for each gene of interest, zMADM enables studies of all genes between the zMADM locus and the telomere on that chromosome arm using simple CRISPR/Cas9-guided mutagenesis. Importantly, CRISPR is the best way to mutate genes that reside near the zMADM cassettes, because it would take thousands or even more zebrafish for one meiotic recombination event between closely linked loci. Finally, it should be noted that our observed overexpansion of nf1-null cells could result from either of two alternative ways: 1) passive expansion, mutant cells proliferate more rapidly or longer without affecting the wild-type cells, or 2) active expansion, the proliferation of mutant cells leads to the death of wild-type cells. Since the key to tease apart these two possibilities is the outcome of wild-type cells, conventional

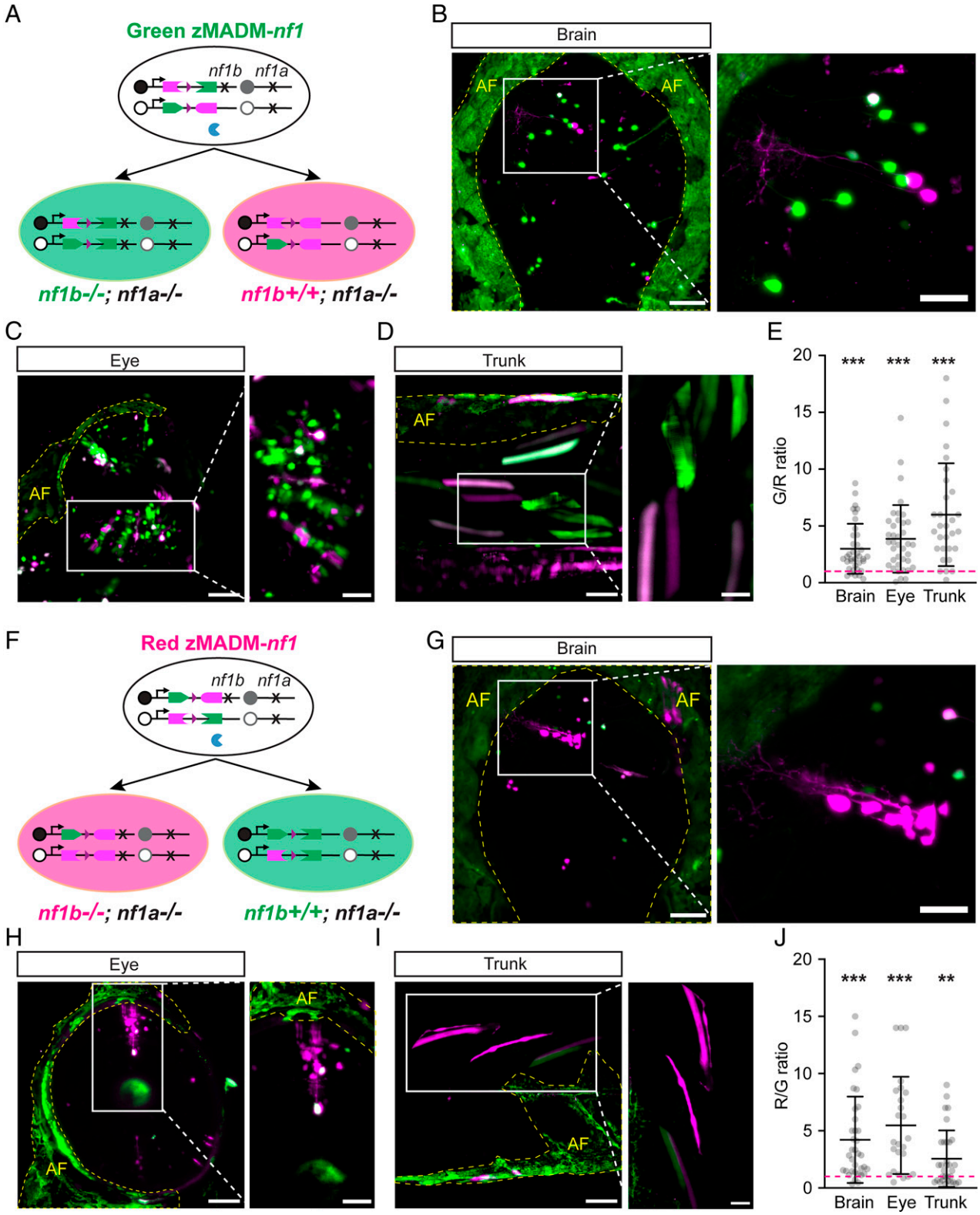

Fig. 4. Phenotypic analysis in zMADM-*nf1* zebrafish. (*A*) The schematic of green zMADM-nf1, in which *nf1b* mutation links to zMADM-AG in a *nf1a*-null background. (*B–D*) Representative confocal images of brain (*B*), eye (*C*), and trunk (*D*) in green zMADM-*nf1* zebrafish show more green *nf1*-null cells than red wild-type cells. The regions in the yellow dashed lines are autofluorescence (AF) of the skin. (Scale bars: original images, 50 μm; zoom-in images, 25 μm.) (*E*) Quantification shows the G/R ratios in brain, eye, and trunk are significantly higher than 1 (red dashed line) in green zMADM-*nf1* zebrafish. Brain, n = 37; eye, n = 38; trunk, n = 30. Data are mean ± SD. ***$P < 0.001$ (one-sample t and Wilcoxon test). (*F*) The schematic of red zMADM-*nf1*, in which *nf1b* mutation linked to zMADM-GA in a *nf1a*-null background. (*G–I*) Representative confocal images of brain (*G*), eye (*H*), and trunk (*I*) in red zMADM-*nf1* zebrafish show more red *nf1*-null cells than green wild-type cells. The regions in the yellow dashed lines are autofluorescence of the skin. (Scale bars: original images, 50 μm; zoom-in images, 25 μm.) (*J*) Quantification shows the R/G ratios in brain, eye, and trunk are significantly higher than 1 (red dashed line) in red zMADM-nf1 zebrafish. Brain, n = 35; eye, n = 25; trunk, n = 32. Data are mean ± SD. **$P < 0.01$, ***$P < 0.001$ (one-sample t and Wilcoxon test).

CKO models would not work since all cells in the population would be mutant. As a genetic mosaic system, zMADM would be perfect to distinguish these two alternatives: For the former, wild-type cells would remain constant despite the increased number of mutant cells, while for the latter, wild-type cells would continue to decline as mutant cells expand in their number.

Future Improvement of zMADM. We envision that zMADM could be further improved by modifying either the Cre recombinase or the zMADM cassettes to allow temporal control and to enable gain-of-function studies. Leveraging zebrafish embryo transparency, one could use a photocaged analog of Cre recombinase and 405 nm light to catalyze DNA recombination at a desired time (34, 35). Alternatively, Cre fused to a mutated ligand-binding domain of the human estrogen receptor (CreER) can be used to allow temporal control with tamoxifen administration (36, 37). To enable gain-of-function studies, Gal4/UAS and Tet-On binary overexpression systems (38–40) could be incorporated into the zMADM system. Gal4 or rtTA could be fused to the distal part of zMADM cassettes such that, after recombination, Gal4 or rtTA would express in green but not red cells. UAS- or TRE-driven transgenes would then specifically express a gene of interest in green cells, enabling genetic rescue if the KO gene were reexpressed or genetic interaction studies if a different gene were expressed. Finally, it would be of great value to the community to establish zMADM on both arms of all chromosomes in zebrafish so that in vivo functions of most genes could be studied with zMADM.

Applications of zMADM. Lineage tracing is a method to track the fate of cells derived from the same progenitor. Because of embryonic transparency, zebrafish is a good animal model for lineage tracing by direct observation during early embryonic development. Through dye labeling, transgenic reporters, genome editing, single-cell RNA sequencing, and computational analyses, zebrafish has been widely used for lineage tracing from single-cell tracing to the developmental trajectory construction of whole embryos (41–45). Previously, zebrabow and skinbow were developed to trace cell lineages with multiple colors (46, 47). Although these multicolor systems greatly facilitate lineage tracing, especially when the mother cells can produce multiple lineages, they do not allow for the study of gene function during lineage development. In contrast, while zMADM allows only the tracing two lineages, it complements previous systems in two aspects: Green and red cells are sibling cells at a clonal level, and the role of a specific gene in lineage development can be revealed if it resides on the zMADM cassette-bearing chromosome.

Many human diseases, such as developmental disorders, cancers, and neurological diseases, are caused by genetic mosaicism, in which disease-causing cells carry distinct gene mutations from the rest of the body (48, 49). Therefore, genetically engineered mosaic animal models are highly valuable for the study of biological processes and disease mechanisms in multicellular organisms. The mouse MADM system has been used to model human diseases. For example, a MADM-based glioma model revealed oligodendrocyte progenitor cells as a cell of origin of glioma based on comparative analysis between green mutant and red wild-type cells (17). Additionally, a MADM-based medulloblastoma model leveraged MADM's lineage tracing capacity to uncover an intricate tumor-supporting network, in which some tumor cells transdifferentiate into astrocytes to support tumor progression (18). Further, taking advantage of the fact that MADM can generate only green and red cells after cell divisions, the mouse MADM has also been applied to study regenerative biology, such as heart regeneration (50). Building on a rich history of using zebrafish for disease modeling (2, 51) and regenerative biology studies (52, 53), zMADM could provide a powerful tool to delineate the intricate interactions between mutant and environmental cells in real time, revealing key insights for effective disease intervention.

Limitations of zMADM. While the low labeling efficiency of zMADM is highly desirable for clonal analysis, in some cases it could be too low, especially when the target cell population is very small. This limitation could be circumvented by using a strong promoter or Gal4/UAS or rtTA/TetO amplification systems to drive high-level expression of Cre in the target cell type. Finally, due to the transparent body of zebrafish larvae, one could visually screen a large cohort of zebrafish to identify zMADM-labeled larvae for intended studies even if the labeling efficiency is relatively low but within a reasonable range.

According to the design principle of zMADM, it can generate green mutant cells and red wild-type sibling cells only in mitotically active cells, because interchromosomal recombination in postmitotic cells results only in yellow, heterozygous cells. Therefore, while conventional CKO models can study gene functions in both mitotic and postmitotic cells, the zMADM system is limited to be used for mitotic cells. As long as the gene of interest does not affect the developmental process, one could use zMADM to knock out the gene during development and then study the gene's function in the postmitotic cells. If the gene of interest impacts development significantly, one could use the rtTA/TetO system to express a wild-type (WT) allele to rescue developmental defects and then withdraw doxycycline at the desired time to study mutant phenotypes in postmitotic cells. It should be noted that the elav3-Cre used in this study, while known to express in postmitotic cells, most likely had leaky expression in neuronal progenitor cells, resulting in green and red cells.

Finally, the speed of early development could outpace the degradation of mRNAs and proteins of the gene inactivated by zMADM, resulting in the masking of phenotypes. Gene product perdurance is an intrinsic problem while studying early development and not specific to zMADM. Caution should be taken while interpreting data during this time window.

Materials and Methods

Zebrafish Husbandry. All animal studies were approved by The University of Virginia Institutional Animal Care and Use Committee (Protocol 3782). *nf1a; nf1b* mutant zebrafish (32) were used for establishing the mutant zMADM. Adult zebrafish were maintained at 28 °C at a density of 8 to 10 fish per liter. Zebrafish embryos were produced by pairwise mating, raised at 28.5 °C in 10-cm Petri dishes filled with egg water (6 g Instant Ocean/20 L RO water), and staged by dpf. Embryos used for live imaging after 24 hpf were treated with 0.004% phenylthiourea (PTU) in egg water to reduce pigmentation. Embryos and larvae were anesthetized using 3-aminobenzoic acid ester (Tricaine). Euthanasia was done with an overdose of Tricaine.

Microinjection. The day before the microinjection, the zebrafish were pairwise separated by divider in the same breeding tank. On the day of microinjection, the divider was removed for the generation of the fertilized eggs. The embryos were aligned on the mold to stabilize for injection. One nanoliter of reagents, including 25 ng/μL plasmids and/or 30 ng/μL mRNAs, was injected into the animal pole of the one-cell embryos. After microinjection, embryos were raised at 28.5 °C in 10-mL Petri dishes for the future experiments.

Generation of Knock-in Zebrafish Lines. The knock-in zebrafish lines were generated by the CRISPR/Cas9-mediated knock-in method (54). To screen for the highest-efficiency sgRNAs, we designed five potential sgRNAs targeting the intergenic region between genes *rassf2b* (20,641,001 to 20,650,302) and *kcnip3b* (20,653,716 to 20,706,270) on chromosome 10 (45,420,867) (*SI Appendix*, Fig. S2*A*). Then, 80 pg sgRNAs was coinjected with 500 pg Cas9 proteins into one-cell zebrafish embryos. At 2 dpf, the genomic DNA was extracted from these embryos and the genomic region containing these sgRNA target sites was applied and sequenced. According to the sequencing chromatograms, we identified the highest-efficiency sgRNA with more chaotic peaks. The donor plasmids (*KI-eab2:GA* and *KI-eab2:AG*) containing ~500 bp of genomic regions including the sgRNA targeted site were constructed. A 1-nL mixture of 15 ng/μL donor plasmids, 80 ng/μL sgRNA, and 600 ng/μL zCas9

mRNA was injected into one-cell embryos and grown to adulthood. The putative knock-in founders were identified by PCR screening of embryos collected from the outcross of adult knock-in zebrafish with AB wild-type zebrafish. The stable F2 knock-in zebrafish lines were obtained by crossing F1 adults with AB wild-type zebrafish. We are in the process of depositing all these zMADM lines in the Zebrafish International Resource Center (ZIRC).

The sgRNA sequences were as follows:

sgRNA-1: GCCTTGGACTGCTTATGTAA
sgRNA-2: GTTAATGGTGCAGAACAGAA
sgRNA-3: GTTGCTGGAGGTTGGCTTGA
sgRNA-4: GTGATAAATGGTGATGTTAA
sgRNA-5: GCTTGGACTGCTTATGTAATG.

The primers used for amplifying the genomic sequence containing sgRNA targeted sites were as follows:

sgRNA-test-F: GCTTGGACTGCTTATGTAATG
sgRNA-test-R: TTTCCTTACAGGCCTAAATTTGG.

The primers used for screening were as follows:

F1: GGCCAAATGCAAATACATTCACTC
R1: GCTTGCATGCCTGAGAATTTCAG
F2: GGTTTGTCCAGGAGTTCTTGACAG
R2: GCGAAAAGGGGCAGAGATTACA.

Genotyping. To genotype the zMADM-AG, zMADM-GA, *nf1a*, and *nf1b* mutant zebrafish, the genomic DNA was extracted using the HotSHOT (hot sodium hydroxide and Tris) method (55). The primers used for genotyping *nf1a* and *nf1b* have been published (32). For zMADM-AG and zMADM-GA, PCR was performed using the following primers:

AG-geno-F: GTACGTCCAGGAGCGCACCA
AG-geno-R: GTGGCGGATCTTGAAGTTCGCC
GA-geno-F: TGAGCAAGGGCGAGGAGAATAACA
GA-geno-R: CATCACGCGCTCCCACCTG.

The genotyping products for zMADM-AG and zMADM-GA are 230 and 300 bp.

Imaging. For screening promoters and RFPs and testing intron splicing (Fig. 1), embryos were manually dechorionated at 24 hpf and anesthetized with Tricaine. Then images were taken using a Zeiss AxioObserver Z1 microscope. For imaging zMADM-labeled zebrafish larvae older than 24 hpf, embryos were manually dechorionated at 24 hpf and PTU was added to prevent pigmentation. On the day of imaging, zebrafish larvae were mounted with 0.8% low-melting-point agarose in 35-mm glass-bottom Petri dishes for confocal imaging or a glass capillary for light-sheet confocal microscopy. For imaging whole larvae with zMADM labeling (Fig. 2 *A*–*C*), a tile scan was used with a 10× objective lens (NA = 0.3) on a Zeiss LSM 880. For other imaging and time-lapse imaging of zMADM-labeled cells, a Zeiss Z1 light-sheet confocal microscope equipped with a 20× water objective lens (NA = 1.0) was used. The interval for Fig. 3*A* is 30 min. The interval for Fig. 3 *I* and *J* is 20 min. All images were processed by Fiji (56). Only the brightness and contrast were adjusted.

DAPI Staining and Quantification of Labeling Efficiency. The 24-hpf zMADM embryos were manually dechorionated and treated with 0.004% PTU in egg water to reduce pigmentation and raised to 4 dpf. Then larvae were fixed with 4% paraformaldehyde (PFA) at 4 °C overnight. On the next day, fixed larvae were washed with 0.3% PBT three times and stained with 1 μg/mL DAPI in 0.3% PBT (PBS containing 0.3% Triton-X 100) for 2 h at room temperature in the dark. After washing three times with 0.3% PBT, the larvae were immersed in 0.8% low-melting-point agarose and mounted in 35-mm glass-bottom Petri dishes (Cellvis) for imaging. For each larva, three optic slices were taken to quantify the total number of DAPI- and zMADM-labeled cells. The ImageJ plugin, Image-based Tool for Counting Nuclei (ITCN), was used to count the DAPI number with 15 pixels in width and 6 pixels in minimum distance. zMADM-labeled cells were manually counted. Labeling efficiency was determined by dividing zMADM-labeled cells by total DAPI number.

Immunofluorescence. The 4-dpf larvae were fixed with 4% PFA containing 0.1% TritonX-100 at 4 °C overnight. They were then washed sequentially with 1% PBT (PBS containing 1% TritonX-100) for 5 min and DWT (distilled water with 1% TritonX-100) for 5 min. After washing, 1 mL −20 °C cold acetone was used to treat embryos for 10 min at −20 °C, followed by three washes with PBST for 5 min. Then embryos were then blocked with 5% goat serum/PBT for 1 h at room temperature. The primary antibodies were diluted in the blocking buffer and incubated with the larvae overnight at 4 °C. On the second day, the larvae were washed three times with PBT for 30 min followed by a final wash for 1 h. Secondary antibodies were diluted in blocking buffer and incubated with the larvae overnight at 4 °C. On the third day, larvae were washed three times with PBT for 1 h. After staining, the larvae were ready for imaging. The primary antibodies used were anti-HuC/D (1:500; mouse; catalog no. A21271; ThermoFisher Scientific) and anti-DsRed (1:100; rabbit; catalog no. 632496; Clontech). The secondary antibodies used were Alex 647 donkey anti-mouse (1:500; catalog no. A31571; ThermoFisher Scientific) and Alex 555 donkey anti-rabbit (1:500; catalog no. A31572; ThermoFisher Scientific).

Construction of Plasmids.

pTol2-eab2:eGFP/mApple. The eab2 promoter was released from the *eab2:mcherry* plasmid (21) (provided by Wenbiao Chen) by restriction enzyme digest with XhoI and BamHI and was subsequently inserted into *pTol2-zubi:eGFP* (20) (provided by Weijun Pan) cut with XhoI and BamHI to remove the *zubi* promoter, resulting in *pTol2-eab2:eGFP*. mApple was amplified from *pCS2:mApple* and inserted into *pTol2-eab2:eGFP* to replace the *eGFP* with BamHI and NdeI.

KI-eab2:AA/GG/AG/GA. The three mutually exclusive loxP sites (loxP511, loxP2272, and loxP) were inserted into the β-globin intron used by the mouse MADM system (9). After selection, the loxP-containing intron was inserted into the *mApple*, *eGFP* according to the intron–exon boundary principle. The full sequences of AA, GG, GA, and AG were synthesized by Synbio Technologies flanked with BamHI and NdeI restricted enzymatic sites. Then AA, GG, GA, and AG were inserted into the *pTol2-eab2:eGFP* with BamHI and NdeI to replace the *eGFP* to generate the *pTol2-eab2:AA/GG/AG/GA*. For the knock-in donor, the genomic sequence containing the sgRNA sequence was amplified and inserted into *pTol2-eab2:AA/GG/AG/GA* ahead of the *eab2* promoter with NsiI and XhoI. We are in the process of depositing all these zMADM plasmids to AddGene.

The primers for amplifying the genomic sequence are as follows:

arm-F: CGCATGCATTTCCAGATGAGTTCACCACCC
arm-R: CGCCTCGAGTTTCCTTACAGGCCTAAATTTGG.

pCS2:mApple/mRuby2/mRuby3/TagRFP/mScarlet/Cre. The plasmids containing *mApple/mRuby2/mRuby3/TagRFP/mScarlet* were purchased from AddGene. The sequences of RFPs were amplified from these plasmids and inserted into pCS2 plasmids by BamHI and XbaI. The sequence of Cre was amplified from *pCA(HZ2-FNF):Cre* and inserted into pCS2 plasmid by BglII and XbaI. The primers are as follows:

mApple-F: CGCGGATCCGCCACCATGGTGAGCAAGGGCGAG
mApple-R: CGCTCTAGATTACTTGTACAGCTCGTCCATGC
mRuby2/3-F: CGCGGATCCGCCACCATGGTGAGCAAGGGCGAG
mRuby2/3-R: CGCTCTAGATCACTTGTACAGCTCGTCCATTCC
TagRFP-F: CGCGGATCCGCCACCATGGTGTCTAAGGGCGAAGAG
TagRFP-R: CGCTCTAGATCAATTAAGTTTGTGCCCCAG
mScarlet-F: CGCGGATCCGCCACCATGGTGAGCAAGGGCGAG
mScarlet-R: CGCTCTAGATCACTTGTACAGCTCGTCCATG
Cre-F: CGCAGATCTGCCACCATGGGCCCAAAGAAGAAGAGA
Cre-R: CGCGTCGACTCTAGACTAATCGCCATCTTCCAGCAG.

pTol2-eab2:Cre. *Cre* was amplified from *pCS2:Cre* and inserted into *pTol2-eab2:eGFP* by BglII and NdeI.

pTol2-elval3:Cre. *Cre* was amplified from *pCS2:Cre* and inserted into *pTol2-elval3:GCaMP6s* (purchased from AddGene) with XmaI.

pTol2-kdrl:Cre. *p5E:kdrl* was purchased from AddGene. The *eab2* promoter in *pTol2-eab2:eGFP* was replaced by the *kdrl* promoter by XhoI and BamHI to generate the *pTol2-kdrl:eGFP*. Then the *Cre* was amplified from *pCS2:Cre* and inserted into *pTol2-kdrl:eGFP* with BglII and HpaI.

In Vitro Transcription. For the transcription of RFPs, *Tol2*, and *Cre* mRNA, plasmids were linearized by NotI. After purification, about 1 μg plasmids was used for in vitro transcription by the mMESSAGE mMACHINE SP6 Transcription Kit (catalog no. AM1340; ThermoFisher Scientific). The mRNAs were aliquoted and stored at −80 °C for long-term storage. The *Tol2* mRNA was transcribed by *pCS2:TP* plasmids (provided by Jiulin Du). For transcription of *zCas9* mRNA, the *pGH-T7:zCas9* plasmids (24) (provided by Jiulin Du) were linearized by XbaI. After purification, about 1 μg plasmids was used for in vitro transcription by the mMESSAGE mMACHINE T7 ULTRA Transcription Kit (catalog no. AM1345; ThermoFisher Scientific). The mRNA was aliquoted and stored at −80 °C for long-term storage. For the transcription of sgRNA, the T7-sgRNA was amplified by primers from *pT7:sgRNA* plasmids (24) (provided by Jiulin Du) and purified. Then 0.5 to 1 μg T7-sgRNA was used for in vitro transcription by the MAXIscript T7 Transcription Kit (catalog no. AM1314; ThermoFisher

Scientific). After the transcription, the sgRNA was isolated by the mirVana miRNA Isolation Kit, without phenol (catalog no. AM1561; ThermoFisher Scientific). The sgRNA was aliquoted and stored at −80 °C for long-term storage.

The primers for amplifying the T7-sgRNA are as follows:

T7-sgRNA-F: GAAATTAATACGACTCACTATA
T7-sgRNA-R: AAAAAAAGCACCGACTCGGTGCCAC.

Statistical Analysis. All data were analyzed using GraphPad Prism 8. All of the data are mean ± SD. An unpaired Student's *t* test was used to compare eGFP intensities (Fig. 1*E*). A paired Student's *t* test was used to compare green and red cell numbers in mixed-labeled neuronal columns (Fig. 3*H*). One-way ANOVA followed by Dunnett's multiple-comparisons test was used to assess differences in RFP intensity (Fig. 1*F*). One-way ANOVA followed by Tukey's multiple-comparisons test was used to compare cell numbers of green, red, and yellow cells in *Cre* mRNA- or *eab2:Cre* plasmid-injected zMADM zebrafish (Fig. 2 *E* and *F*) and the percentage of green, red, and mixed neuronal columns (Fig. 3*G*). One sample *t* test was used to compare the difference of G/R (Fig. 4*E*) and R/G (Fig. 4*J*) ratio in zMADM-*nf1* zebrafish with 1 (theoretical G/R and R/G ratio in wild-type zMADM zebrafish).

Data Availability. Plasmids (catalog numbers: pTol2-eab2-AA: 182153; pTol2-eab2-GG: 182154; pTol2-eab2-AG: 182155; pTol2-eab2-GA: 182156; KI-eab2-AA: 182157; KI-eab2-GG: 182158; KI-eab2-AG: 182159; KI-eab2-GA: 182160) have been deposited to AddGene. zMADM fish lines have been deposited in Zebrafish International Resource Center (ZIRC) (http://zebrafish.org).

ACKNOWLEDGMENTS. We thank Kryn Stankunas, Jiandong Liu, Xiaorong Liu, Jingli Cao, Jiulin Du, Yonghua Sun, and Adam Miller for critical discussions and insightful feedback on our manuscript and Lori Tocke for technical support in the zebrafish facility. We thank Dr. Wenbiao Chen at Vanderbilt University for the generous sharing of the *eab2* promoter, Dr. Jiulin Du at Center for Excellence in Brain Science and Intelligence Technology, Chinese Academy of Sciences for the generous sharing of the *pCS2:TP, pGH-T7:zCas9* and *pT7:sgRNA* plasmids, and Dr. Weijun Pan at Shanghai Institute of Nutrition and Health, Chinese Academy of Sciences for the generous sharing of the *zubi:eGFP* plasmid. We acknowledge the University of Virginia (UVa) Keck Center for zebrafish imaging with the Zeiss Z1 light-sheet microscopy system and the UVa Advanced Microscopy Facility for confocal imaging. This project was partially supported by the NIH Office of the Director Grant R21OD026524 (to H.Z.), a UVa School of Medicine Office for Research seed grant (to H.Z.), and UVa Cancer Center Support Grant P30 CA044579.

1. N. G. Holtzman, M. K. Iovine, J. O. Liang, J. Morris, Learning to fish with genetics: A primer on the vertebrate model *Danio rerio*. *Genetics* **203**, 1069–1089 (2016).
2. C. Santoriello, L. I. Zon, Hooked! Modeling human disease in zebrafish. *J. Clin. Invest.* **122**, 2337–2343 (2012).
3. R. Sertori, M. Trengove, F. Basheer, A. C. Ward, C. Liongue, Genome editing in zebrafish: A practical overview. *Brief. Funct. Genomics* **15**, 322–330 (2016).
4. W. Li *et al.*, One-step efficient generation of dual-function conditional knockout and geno-tagging alleles in zebrafish. *eLife* **8**, e48081 (2019).
5. J. Li *et al.*, One-step generation of zebrafish carrying a conditional knockout-knockin visible switch via CRISPR/Cas9-mediated intron targeting. *Sci. China Life Sci.* **63**, 59–67 (2020).
6. L. Burg *et al.*, Conditional mutagenesis by oligonucleotide-mediated integration of loxP sites in zebrafish. *PLoS Genet.* **14**, e1007754 (2018).
7. L. A. Maddison, J. Lu, W. Chen, Generating conditional mutations in zebrafish using gene-trap mutagenesis. *Methods Cell Biol.* **104**, 1–22 (2011).
8. T. Lee, L. Luo, Mosaic analysis with a repressible cell marker for studies of gene function in neuronal morphogenesis. *Neuron* **22**, 451–461 (1999).
9. H. Zong, J. S. Espinosa, H. H. Su, M. D. Muzumdar, L. Luo, Mosaic analysis with double markers in mice. *Cell* **121**, 479–492 (2005).
10. S. L. Lai, T. Lee, Genetic mosaic with dual binary transcriptional systems in Drosophila. *Nat. Neurosci.* **9**, 703–709 (2006).
11. P. Gao *et al.*, Deterministic progenitor behavior and unitary production of neurons in the neocortex. *Cell* **159**, 775–788 (2014).
12. S. Hippenmeyer *et al.*, Genetic mosaic dissection of Lis1 and Ndel1 in neuronal migration. *Neuron* **68**, 695–709 (2010).
13. C. H. Lee, T. Herman, T. R. Clandinin, R. Lee, S. L. Zipursky, N-cadherin regulates target specificity in the Drosophila visual system. *Neuron* **30**, 437–450 (2001).
14. A. Packard *et al.*, Luminal mitosis drives epithelial cell dispersal within the branching ureteric bud. *Dev. Cell* **27**, 319–330 (2013).
15. R. Lasrado *et al.*, Lineage-dependent spatial and functional organization of the mammalian enteric nervous system. *Science* **356**, 722–726 (2017).
16. R. A. Pagliarini, T. Xu, A genetic screen in Drosophila for metastatic behavior. *Science* **302**, 1227–1231 (2003).
17. C. Liu *et al.*, Mosaic analysis with double markers reveals tumor cell of origin in glioma. *Cell* **146**, 209–221 (2011).
18. M. Yao *et al.*, Astrocytic trans-differentiation completes a multicellular paracrine feedback loop required for medulloblastoma tumor growth. *Cell* **180**, 502–520.e19 (2020).
19. X. Contreras *et al.*, A genome-wide library of MADM mice for single-cell genetic mosaic analysis. *Cell Rep.* **35**, 109274 (2021).
20. C. Mosimann *et al.*, Ubiquitous transgene expression and Cre-based recombination driven by the ubiquitin promoter in zebrafish. *Development* **138**, 169–177 (2011).
21. E. J. Boniface, J. Lu, T. Victoroff, M. Zhu, W. Chen, FIEx-based transgenic reporter lines for visualization of Cre and Flp activity in live zebrafish. *Genesis* **47**, 484–491 (2009).
22. N. C. Shaner *et al.*, Improving the photostability of bright monomeric orange and red fluorescent proteins. *Nat. Methods* **5**, 545–551 (2008).
23. R. Marisca *et al.*, Functionally distinct subgroups of oligodendrocyte precursor cells integrate neural activity and execute myelin formation. *Nat. Neurosci.* **23**, 363–374 (2020).
24. B. Xu *et al.*, Neurons secrete miR-132-containing exosomes to regulate brain vascular integrity. *Cell Res.* **27**, 882–897 (2017).
25. K. Kretzschmar, F. M. Watt, Lineage tracing. *Cell* **148**, 33–45 (2012).
26. S. R. Cooper *et al.*, Protocadherins control the modular assembly of neuronal columns in the zebrafish optic tectum. *J. Cell Biol.* **211**, 807–814 (2015).
27. X. Qian, S. K. Goderie, Q. Shen, J. H. Stern, S. Temple, Intrinsic programs of patterned cell lineages in isolated vertebrate CNS ventricular zone cells. *Development* **125**, 3143–3152 (1998).
28. G. A. Pilz *et al.*, Live imaging of neurogenesis in the adult mouse hippocampus. *Science* **359**, 658–662 (2018).
29. C. M. Niell, S. J. Smith, Functional imaging reveals rapid development of visual response properties in the zebrafish tectum. *Neuron* **45**, 941–951 (2005).
30. K. Cichowski, T. Jacks, NF1 tumor suppressor gene function: Narrowing the GAP. *Cell* **104**, 593–604 (2001).
31. G. Bollag *et al.*, Loss of NF1 results in activation of the Ras signaling pathway and leads to aberrant growth in haematopoietic cells. *Nat. Genet.* **12**, 144–148 (1996).
32. J. Shin *et al.*, Zebrafish neurofibromatosis type 1 genes have redundant functions in tumorigenesis and embryonic development. *Dis. Model. Mech.* **5**, 881–894 (2012).
33. R. T. Collins, C. Linker, J. Lewis, MAZe: A tool for mosaic analysis of gene function in zebrafish. *Nat. Methods* **7**, 219–223 (2010).
34. W. Brown, J. Liu, M. Tsang, A. Deiters, Cell-lineage tracing in zebrafish embryos with an expanded genetic code. *ChemBioChem* **19**, 1244–1249 (2018).
35. W. Brown, A. Deiters, Light-activation of Cre recombinase in zebrafish embryos through genetic code expansion. *Methods Enzymol.* **624**, 265–281 (2019).
36. R. Feil *et al.*, Ligand-activated site-specific recombination in mice. *Proc. Natl. Acad. Sci. U.S.A.* **93**, 10887–10890 (1996).
37. S. Hans, J. Kaslin, D. Freudenreich, M. Brand, Temporally-controlled site-specific recombination in zebrafish. *PLoS One* **4**, e4640 (2009).
38. M. E. Halpern *et al.*, Gal4/UAS transgenic tools and their application to zebrafish. *Zebrafish* **5**, 97–110 (2008).
39. K. Kawakami *et al.*, Gal4 driver transgenic zebrafish: Powerful tools to study developmental biology, organogenesis, and neuroscience. *Adv. Genet.* **95**, 65–87 (2016).
40. F. Knopf *et al.*, Dually inducible TetON systems for tissue-specific conditional gene expression in zebrafish. *Proc. Natl. Acad. Sci. U.S.A.* **107**, 19933–19938 (2010).
41. C. B. Kimmel, R. M. Warga, Tissue-specific cell lineages originate in the gastrula of the zebrafish. *Science* **231**, 365–368 (1986).
42. P. J. Keller, A. D. Schmidt, J. Wittbrodt, E. H. Stelzer, Reconstruction of zebrafish early embryonic development by scanned light sheet microscopy. *Science* **322**, 1065–1069 (2008).
43. J. A. Farrell *et al.*, Single-cell reconstruction of developmental trajectories during zebrafish embryogenesis. *Science* **360**, eaar3131 (2018).
44. A. McKenna *et al.*, Whole-organism lineage tracing by combinatorial and cumulative genome editing. *Science* **353**, aaf7907 (2016).
45. D. E. Wagner *et al.*, Single-cell mapping of gene expression landscapes and lineage in the zebrafish embryo. *Science* **360**, 981–987 (2018).
46. C. H. Chen *et al.*, Multicolor cell barcoding technology for long-term surveillance of epithelial regeneration in zebrafish. *Dev. Cell* **36**, 668–680 (2016).
47. Y. A. Pan *et al.*, Zebrabow: Multispectral cell labeling for cell tracing and lineage analysis in zebrafish. *Development* **140**, 2835–2846 (2013).
48. L. G. Biesecker, N. B. Spinner, A genomic view of mosaicism and human disease. *Nat. Rev. Genet.* **14**, 307–320 (2013).
49. A. Poduri, G. D. Evrony, X. Cai, C. A. Walsh, Somatic mutation, genomic variation, and neurological disease. *Science* **341**, 1237758 (2013).
50. T. M. A. Mohamed *et al.*, Regulation of cell cycle to stimulate adult cardiomyocyte proliferation and cardiac regeneration. *Cell* **173**, 104–116.e12 (2018).
51. G. J. Lieschke, P. D. Currie, Animal models of human disease: Zebrafish swim into view. *Nat. Rev. Genet.* **8**, 353–367 (2007).
52. K. D. Poss, L. G. Wilson, M. T. Keating, Heart regeneration in zebrafish. *Science* **298**, 2188–2190 (2002).
53. C. Jopling *et al.*, Zebrafish heart regeneration occurs by cardiomyocyte dedifferentiation and proliferation. *Nature* **464**, 606–609 (2010).
54. J. Li *et al.*, Intron targeting-mediated and endogenous gene integrity-maintaining knockin in zebrafish using the CRISPR/Cas9 system. *Cell Res.* **25**, 634–637 (2015).
55. G. E. Truett *et al.*, Preparation of PCR-quality mouse genomic DNA with hot sodium hydroxide and tris (HotSHOT). *Biotechniques* **29**, 52, 54 (2000).
56. J. Schindelin *et al.*, Fiji: An open-source platform for biological-image analysis. *Nat. Methods* **9**, 676–682 (2012).